

## The usage of magnesite production wastes in ceramic tile bodies

Gülfem Binal<sup>a,\*</sup> and Nuran Ay<sup>b</sup>

<sup>a</sup>Bartın University, Faculty of Engineering, Department of Metallurgical and Materials Engineering, 74100, Bartın, Turkey

<sup>b</sup>Anadolu University, Faculty of Engineering, Department of Material Science and Engineering, İki Eylül Campus, 26555, Eskisehir, Turkey

In this study the possibility of using magnesite wastes, which were consist of during the production of magnesite from Tutluca village (southwest of Eskisehir/Turkey) ore bed to make ceramic tile bodies were explored. The magnesite deposits of Tutluca village lie in serpentized harzburgites and dunites of Alpine type ultramafic rocks. The features of magnesite production wastes were investigated by applying thermal analysis, X-ray diffraction and X-ray fluorescence spectroscopy. Examined magnesite wastes were added to ceramic tile body compositions in different amounts (20-80 wt.%). Prepared ceramic tile samples were sintered in a laboratory type fast firing kiln at firing temperature and cycle of 1165 °C for 37 minute. Linear firing shrinkage, water absorption, firing strength and porosity values of the resultant products were measured as a function of increasing magnesite waste content. XRD and SEM analysis of resultant products were also investigated. As a result of this study, it has been seen that magnesite production wastes can be utilized as an alternative raw materials for production of ceramic tile with the properties in accordance with wall tiles.

**Key words:** Magnesite production wastes, Ceramic tile, Forsterite, Enstatite.

### Introduction

The proliferation of the world's population increases the consumption of construction building materials. The growth of consumption and consequently the increase in industrial production have led to a rapid decrease in available natural sources (raw materials and sources of energy). On the other hand a large amount of industrial waste and sub-products were comprised and most of them could not recycled [1]. Compositions of traditional clay-based ceramic products, produced from natural raw materials, varies over a wide range, therefore these products can tolerate changes in raw materials and it is possible to use greater amounts of various waste materials [1-3].

Magnesite is an important raw material for refractory industry. However, magnesite mining and processing both generate large amounts of waste like rocks and side stones removed from the environment. Characteristic side stones of magnesite are serpentines, dolomite, biotite, Gröna, talc quartz and opal. Serpentine minerals are belongs to the group of sheet silicates (phyllosilicates) like micas, chlorite, talc, and the clay minerals. Chrysotile, lizardite and antigorite are the most common types of rock-forming serpentine minerals. These minerals are described as being trioktahedrik (1 : 1), layered silicates, having the general chemical formula  $Mg_3Si_2O_5(OH)_4$  [4].

In serpentine minerals silicon-tetrahedra are shared three out of four apical oxygen atoms with the other tetrahedra. Unshared oxygen atoms are bonded to Mg atoms of the octahedral sheet [5]. The chemical composition of serpentine is approximately in the form of 43% MgO, 44.1% SiO<sub>2</sub>, and 12.9% H<sub>2</sub>O.

In this study, magnesite wastes that occur during the production of magnesite from the ore bed were added to ceramic tile bodies and the effect of addition on the properties of the final product were examined.

### Experimental Procedure

In the experiments, magnesite production wastes, clays and pegmatite were used. The chemical composition of raw materials and wastes were analyzed by XRF (Rigaku ZSX Primus) and results are given in Table 1.

Thermal analyses of magnesite host rocks (TG, DTA) were carried out in air using a Netzsch STA 409 PC/PG instrument and a heating rate of 20 °C min<sup>-1</sup> up to 1200 °C. The X-ray diffractogram of the powdered wastes and fired tiles was recorded with Rigaku, Rint 2000 X-ray Diffraction spectrometer using Cu K $\alpha$  radiation at 40 kV accelerating voltage and 30mA current in 5-70 ° 2 $\theta$  range.

Ceramic tile recipes in the form of R-coded prescriptions are given in Table 2. Ceramic tile mixtures were wet-ground in a ball mill until the residue on a 63  $\mu$ m sieve was reduced to 3-3.6%. The slips were dried, deagglomerated and humidified (6 wt.% moisture content). The humidified powders were pressed in size 100 × 50 × 5 mm specimens with using 360 kg/cm<sup>2</sup> forming pressure (Gabbrielli

\*Corresponding author:  
Tel : +90-378-223-53-56  
Fax: +90-378-223-52-58  
E-mail: gbinal@bartin.edu.tr

**Table 1.** Chemical composition of raw materials and wastes (wt.%).

|                                | Sandy Clay | Clay 1 | Clay 2 | Clay3 | Pegmatite | Waste |
|--------------------------------|------------|--------|--------|-------|-----------|-------|
| SiO <sub>2</sub>               | 77.02      | 64.59  | 59.93  | 58.63 | 73.54     | 25.75 |
| Al <sub>2</sub> O <sub>3</sub> | 11.09      | 20.79  | 21.14  | 24.72 | 16.96     | 0.73  |
| Fe <sub>2</sub> O <sub>3</sub> | 2.58       | 2.72   | 4.83   | 3.34  | 1.10      | 6.26  |
| TiO <sub>2</sub>               | 0.54       | 1.14   | 1.15   | 1.63  | 0.57      | –     |
| CaO                            | 1.32       | 0.17   | 0.30   | 0.27  | 0.21      | 2.30  |
| MgO                            | 0.65       | 0.56   | 0.83   | 0.85  | 0.28      | 40.37 |
| Na <sub>2</sub> O              | 0.95       | 0.11   | 0.24   | 0.23  | 0.89      | 0.04  |
| K <sub>2</sub> O               | 1.89       | 2.16   | 3.87   | 2.35  | 1.26      | –     |
| CuO                            | –          | –      | –      | –     | –         | 0.10  |
| NiO                            | –          | –      | –      | –     | –         | 0.25  |
| MnO                            | –          | –      | –      | –     | –         | 0.10  |
| Cr <sub>2</sub> O <sub>3</sub> | –          | –      | –      | –     | –         | 0.34  |
| SO <sub>3</sub>                | –          | –      | –      | –     | –         | 0.16  |
| Loss on ignition               | 3.93       | 7.63   | 8.57   | 7.96  | 5.71      | 23.67 |

**Table 2.** Ceramic tile body recipes (wt.%).

| Raw Materials | Recipe code |    |    |    |    |    |    |
|---------------|-------------|----|----|----|----|----|----|
|               | R1          | R2 | R3 | R4 | R5 | R6 | R7 |
| Pegmatite     | 25          | 23 | 23 | 23 | 13 | 3  | –  |
| Sandy Clay    | 28          | 26 | 10 | –  | –  | –  | –  |
| Clay 1        | 5           | 5  | 5  | 5  | 5  | 5  | –  |
| Clay 2        | 10          | 10 | 10 | 10 | 10 | 10 | 10 |
| Clay 3        | 12          | 12 | 12 | 12 | 12 | 12 | 10 |
| Waste         | 20          | 25 | 40 | 50 | 60 | 70 | 80 |

Press). The dried tiles were fired in laboratory conditions at 1165 °C using a fast-sintering cycle of 37 minute (cold-to-cold).

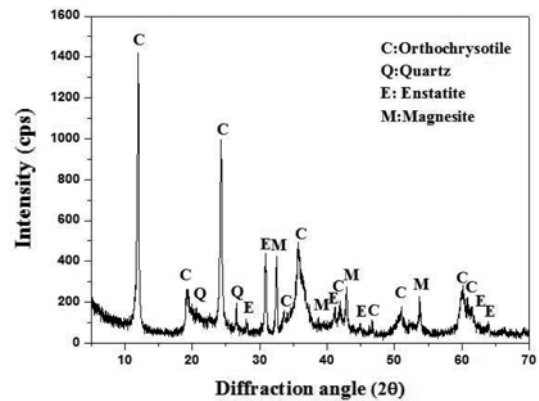
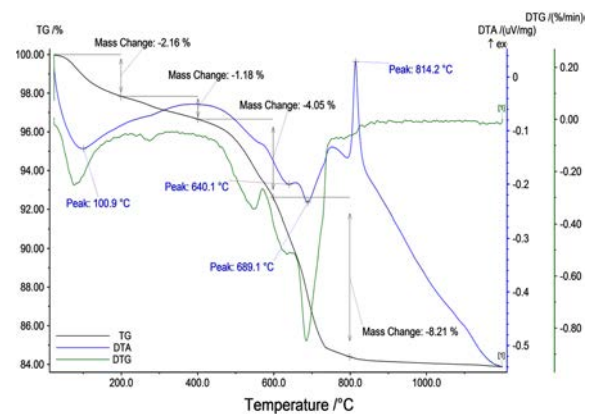
Fired tiles were characterized by the measurement of linear firing shrinkage, water absorption, porosity and the firing strength. The dimensions of the pressed specimens were measured before and after firing in order to determine the firing shrinkage. The water absorption values determined according to ISO 10545-Part 3 [7], porosity values are calculated by Archimedes principles and firing strength of the samples were measured according to ISO 10545-Part 4 [6].

Microstructural examinations and EDS analysis were performed on fracture surfaces of selected fired samples using a scanning electron microscope (SEM) (Zeiss, SUPRA 50 VP) in secondary electron (SE) imaging mode. The surfaces of SEM samples were etched for 35 seconds with %5 hydrofluoric acid (HF) solution and sputtered with a thin layer of gold-palladium alloy.

## Results and Discussion

### Characterization of wastes

XRD spectrum of magnesite production wastes are

**Fig. 1.** XRD spectrum of magnesite production wastes.**Fig. 2.** TG/DTA curves of magnesite production wastes.

shown in Fig. 1. According to XRD spectra magnesite wastes contained orthochrysotile (JCPDS No: 046-1445), quartz (JCPDS No: 046-1045), magnesite (JCPDS No: 008-0479), and enstatite (JCPDS No: 019-0768) phases. The main crystalline phase is orthochrysotile which is one of serpentine polymorphs.

Thermal properties of magnesite wastes were determined by TG/DTA analysis. TG/DTA curves are shown in Fig. 2. It can be seen that the sample exhibits three characteristic endothermic peaks at 100.9, 640.1 and 689.1 °C. The first endothermic peak (mass loss 2.16%) is due to removal of physically adsorbed water. The second and third endothermic peaks (mass loss 12.26%) are due to the removal of hydroxyl groups from serpentine minerals. These endothermic peaks are occurred due to the formation of intermediate phases during dehydration [5, 8-11]. During the dehydration reaction of chrysotile the water molecules are liberated and Mg-O-Si and Si-O-Si bonds are broken. Mg and Si ions begin to migrate in opposite directions thus Mg-rich (phase I) and Si-rich (phase II) regions are formed. Forsterite crystallization takes place from the ordering of Mg-rich regions. Enstatite crystallizes in the Si-rich regions [5, 12]. The exothermic peak at 814.2 °C is due to structural reorganization within the serpentine minerals. According to [13] this exothermic peak is related to the crystallization of forsterite and enstatite which is shown

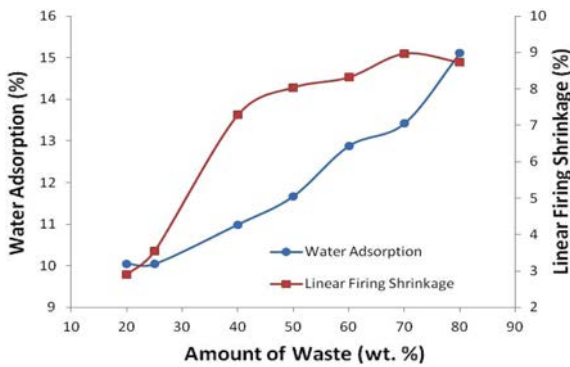


Fig. 3. Variation in water adsorption and linear firing shrinkage values in relation to waste content.

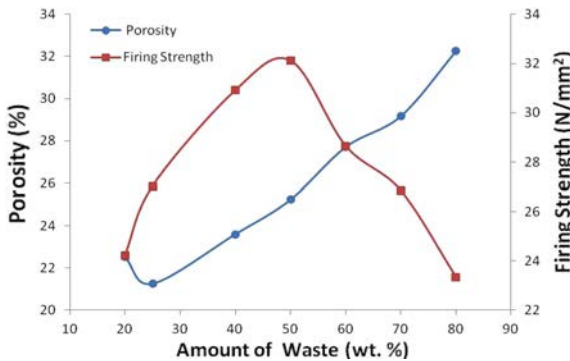
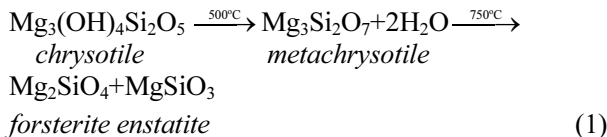


Fig. 4. Variation in porosity and firing strength values in relation to waste content.

in Equation 1.



**Physical properties of ceramic tiles**

Fig. 3 presents the water absorption and linear firing shrinkage values of prepared ceramic tiles according to Table 2. As it can be seen, the water absorption and linear firing shrinkage values increased with increasing amount of magnesite waste. Martin [10], investigated the decomposition of chrysotile by using transmitted electron microscopy and reported that large cavities opened within the chrysotile fiber wall and extended along the fibers because of water loss. During sintering porosity was increased with the addition of waste and the composed liquid phase was not sufficient to reduce porosity. Reduction in pegmatite and clay content of the system due to the increasing amount of waste reduces amount of liquid phase. Therefore pores could not close down and the water absorption values have increased.

The results of the porosity and firing strength tests, as a function of waste content, are given in Fig. 4. The firing strength values increased up to 50 wt.% waste addition. The presence of forsterite and enstatite phases

increases the strength of bodies (Fig. 5). Forsterite and enstatite phases promotes sintering and improves mechanical strength and abrasion resistance in ceramic bodies [14]. Forsterite has good characteristic properties such as low expansion, low thermal conductivity and high volume stability [15]. Due to these characteristics forsterite and enstatite are desirable phases in fired bodies. Waste added in quantities beyond 50 wt.% decreased firing strength of bodies depending on the increment of porosity values.

XRD spectrums of waste containing fired bodies are shown in Fig. 5. Quartz (JCPDS No: 046-1045), forsterite (JCPDS No: 034-0189) and enstatite (JCPDS No: 019-0768) phases has been identified in all samples. Forsterite and enstatite phases in waste containing bodies were formed as a result of chrysotile dehydration and interaction with amorphous SiO<sub>2</sub>. The resulting crystalline phase quantities are determined by using MAUD (Materials Analysis Using Diffraction) program

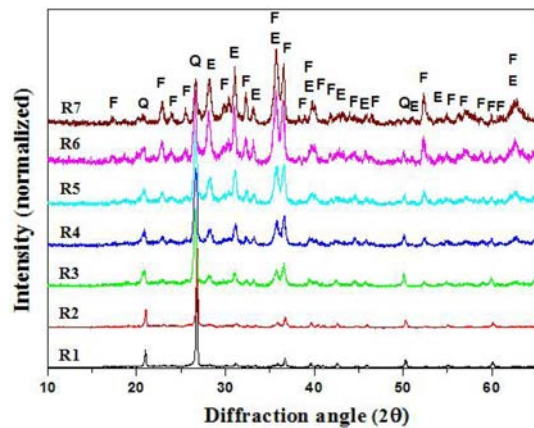


Fig. 5. XRD spectrum of fired samples (F: Forsterite, E: Enstatite, Q: Quartz).

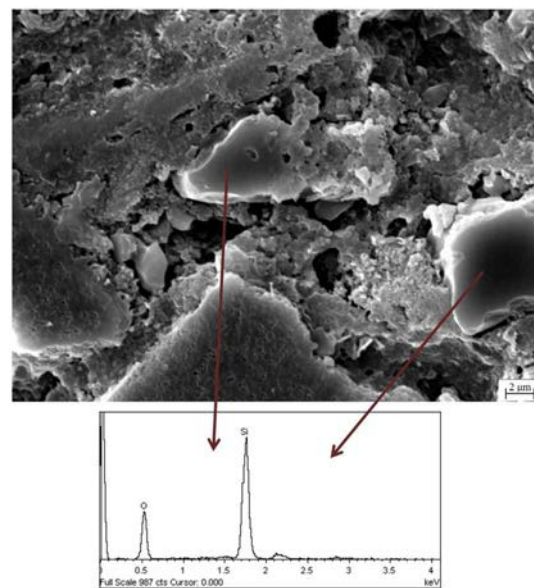
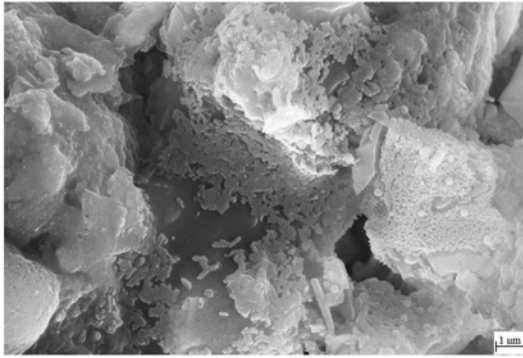
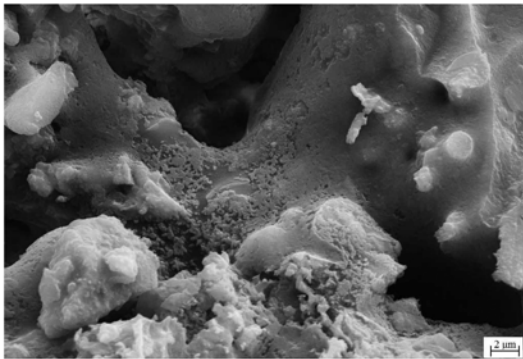


Fig. 6. Representative SEM image (secondary electrons) of R1 coded sample and EDX analysis of quartz crystals.



**Fig. 7.** Representative SEM image (secondary electrons) of R3 coded sample.



**Fig. 8.** Representative SEM image (secondary electrons) of R4 coded sample.

**Table 3.** Quantitative phase compositions of fired samples (wt.%).

| Samples | Enstatite    | Forsterite   | Quartz       | Glassy phase |
|---------|--------------|--------------|--------------|--------------|
| R1      | 4.89 ± 0.33  | 2.53 ± 0.24  | 49.14 ± 0.42 | 43.42 ± 2.77 |
| R2      | 7.24 ± 0.38  | 3.15 ± 0.27  | 48.22 ± 0.42 | 41.39 ± 1.77 |
| R3      | 30.29 ± 1.07 | 4.83 ± 0.32  | 33.83 ± 0.43 | 31.04 ± 1.42 |
| R4      | 32.32 ± 0.73 | 7.17 ± 0.34  | 33.37 ± 0.48 | 27.13 ± 1.17 |
| R5      | 36.80 ± 0.70 | 8.15 ± 0.35  | 26.68 ± 0.48 | 28.37 ± 1.13 |
| R6      | 49.29 ± 1.02 | 7.61 ± 0.39  | 15.90 ± 0.45 | 27.18 ± 1.38 |
| R7      | 49.57 ± 0.71 | 28.43 ± 0.51 | 6.51 ± 0.15  | 15.47 ± 0.56 |

based on the Rietveld method. According to Rietveld analyses when the waste content was increased, the amount of glassy phase and residual quartz decreased; the amount of forsterite and enstatite increased (Table 3). The amount of enstatite is greater than the amount of forsterite. At higher temperatures amorphous silica from clays, pegmatite and waste combines with forsterite to form enstatite crystals. This may explain why the samples demonstrates higher amount of enstatite. There are studies in the literature about chrysotile dehydration which are showing enstatite crystallization via forsterite and amorphous silica reaction at higher temperatures ( $T > 1000\text{ }^{\circ}\text{C}$ ) [5, 11, 12].

Secondary electron images taken from the etched fracture surfaces of selected fired samples are presented in Figs. 6-8. Fig. 6 shows the microstructure of 20 wt.% waste containing R1 body. Quartz grains can be seen in

microstructure. The other crystals are thought to be forsterite and enstatite crystals. As it can be seen from Fig. 7 and Fig. 8 large pores occurs with the addition of increasing amount of waste. Enstatite and forsterite crystals are developed on pores and the glassy phase. Forsterite and enstatite crystals could not be distinguished from each other in SEM images. A large part of forsterite crystals were transformed to enstatite crystals (Table 3) due to high amorphous silica content of ceramic tile samples. Therefore the majority of the crystals are thought to be enstatite. According to some authors forsterite and enstatite grains are difficult to distinguish by SEM due to inter growth of these crystals and grain size below SEM resolution limits [5, 16]. In a study, chrysotile fibers were subjected to heat treatment at different temperatures up to  $1300\text{ }^{\circ}\text{C}$  and examined by TEM. It has been observed that, at  $650\text{ }^{\circ}\text{C}$  flaky forsterite nuclei appeared inside the fibrils, at  $1000\text{ }^{\circ}\text{C}$  very small enstatite grains were developed mixed with forsterite grains. Grain growth was occurred between  $1100\text{-}1300\text{ }^{\circ}\text{C}$  [17].

## Conclusions

The present study demonstrated that

1. The ceramic tiles prepared by using magnesite production waste up to 80 wt.% satisfied the requirements of the ISO 10545 Standard for ceramic wall tiles. According to this results waste can be used as an alternative raw material in ceramic tile bodies.
2. Quartz, forsterite and enstatite phases have been identified in all ceramic tile samples. Forsterite and enstatite phases promote sintering and mechanical strength in ceramic bodies.
3. Magnesite production wastes are disposed at a controlled landfill. The use of magnesite waste in ceramic tile bodies rather than disposal is very important in terms of waste recycling. Waste utilization reduces the consumption of natural raw materials and provides economical and environmental advantages.

## References

1. J.M.F. Ferreira, P.M.C. Torres, M.S. Silva and J.A. Labrincha, Euroceram News. 14 (2002) 1-4.
2. R.R. Menezes, L.N.L. Santana, G.A. Neves and H.C. Ferreira, (2012), Recycling of mine wastes as ceramic raw materials: An alternative to avoid environmental contamination, Environmental Contamination, Jatin Kumar Srivastava (Ed.), ISBN: 978-953-51-0120-8, InTech.
3. A.M. Segades, Advances in Applied Ceramics. 105 (2006) 46-54.
4. G. Gürtekin and M. Albayrak, MTA Dergisi. 133 (2006) 37-46.
5. A.F. Gualtieri, C. Giacobbe and C. Viti, American Mineralogist. 97 (2012) 666-680.
6. ISO 10545-4, Ceramic Tile Part 4, Determination of Modulus of Rupture and Breaking Strength, Switzerland (1997).

7. ISO 10545-3, Ceramic Tile Part 3, Determination of Water Adsorption, Apparent Porosity, Apparent Relative Density and Bulk Density, Switzerland (1997).
8. M.C. Ball and H.F.W. Taylor, *Mineralogical Magazine*. 33 (1963) 467-482.
9. G.W. Brindley and R. Hayami, *Mineralogical Magazine*. 35 (1965) 189-195.
10. C.J. Martin, *Mineralogical Magazine*. 41 (1977) 453-459.
11. H.S. Santos and K. Yada, *Clays and Clay Minerals*. 27 (1979) 161-174.
12. K.J.D. MacKenzie and R.H. Meinhold, *American Mineralogist*. 79 (1994) 43-50.
13. A.F. Gualtieri, and A. Tartaglia, *J. Euro. Ceram. Soc.* 20 (2000) 1409-1418.
14. C. Dagounaki, C. Sikalidis, A. Kassoli-Fournaraki and A. Tsirambides, *Industrial Ceramics*. 28 (2008) 181-187.
15. A.G.M. Othman and N.M. Khalil, *Ceramics International*. 31 (2005) 1117-1121.
16. C. Viti, *American Mineralogist*. 95 (2010) 631-638.
17. H.S. Santos, P.K. Kiyohara and P.S. Santos, *Acta Microscopica*. 4 (1995) 1-10.